SCIENTIFIC REPORTS

OPEN

SUBJECT AREAS:
NANOPARTICLES
TWO-DIMENSIONAL MATERIALS
ELECTRONIC DEVICES
DESIGN, SYNTHESIS AND PROCESSING

Received
18 March 2013

Accepted
24 April 2013

Published
14 May 2013

Correspondence and requests for materials should be addressed to S.F.Y. (Siu.Fung.Yu@inet.polyu.edu.hk) or H.Y.Y. (yanghuiying@sutd.edu.sg)

* These authors contributed equally to this work.

Selective Decoration of Au Nanoparticles on Monolayer MoS_2 Single Crystals

Yumeng Shi[1]*, Jing-Kai Huang[2]*, Limin Jin[3]*, Yu-Te Hsu[2], Siu Fung Yu[3], Lain-Jong Li[2,4] & Hui Ying Yang[1]

[1]Pillar of Engineering Product Development, Singapore University of Technology and Design, Singapore 138682, Singapore, [2]Institute of Atomic and Molecular Sciences Academia Sinica, Taipei 10617, Taiwan, [3]Departments of Applied Physics, the Hong Kong Polytechnic University, Hung Hum, Kowloon, Hong Kong, China, [4]Department of Physics National Tsing Hua University, HsinChu 300, Taiwan.

We report a controllable wet method for effective decoration of 2-dimensional (2D) molybdenum disulfide (MoS_2) layers with Au nanoparticles (NPs). Au NPs can be selectively formed on the edge sites or defective sites of MoS_2 layers. The Au-MoS_2 nano-composites are formed by non-covalent bond. The size distribution, morphology and density of the metal nanoparticles can be tuned by changing the defect density in MoS_2 layers. Field effect transistors were directly fabricated by placing ion gel gate dielectrics on Au-decorated MoS_2 layers without the need to transfer these MoS_2 layers to SiO_2/Si substrates for bottom gate devices. The ion gel method allows probing the intrinsic electrical properties of the as-grown and Au-decorated MoS_2 layers. This study shows that Au NPs impose remarkable *p*-doping effects to the MoS_2 transistors without degrading their electrical characteristics.

Due to their unique properties, atomically thin two-dimensional (2D) materials with a layered structure such as graphene[1–3], hexagonal boron nitride (*h*-BN)[4,5] and transition-metal dichalcogenide (LTMDs)[6–8] have been attracting increasing attention. Molybdenum disulfide (MoS_2), belongs to the layered 2D nanomaterial family, is traditionally used as a solid state lubricant and a catalyst for hydrodesulfurization (HDS) and hydrogen evolution reaction (HER)[9–11]. In recent years, it has been demonstrated that ultra-thin MoS_2 crystals with a typical thickness of ~0.65 nm can be obtained by either physical[6,12] or chemical exfoliation methods[13,14], MoS_2 layers with uniform thickness can also be synthesized in large scale by chemical vapor deposition[15–19]. The monolayer MoS_2 exhibits excellent electrical[6–8] and optical performance[20,21] compared to its bulky counterpart.

MoS_2 can be seen as an inorganic graphene analogue, similar to graphene and *h*-BN. The structure of MoS_2 is based on a hexagonal crystal[22], where Mo atom is six-fold coordinated and hexagonally packed between two trigonally coordinated sulphur atoms. One S-Mo-S quintuple-layer is weakly bonded to another S-Mo-S layer by van der Waals forces. It has been reported that the basal plane of MoS_2 is catalytically inactive, and the activity in the HDS and HER is associated with the edge termination of MoS_2 clusters[9–11,23]. Especially for the MoS_2 nanocrystals form, it has been investigated as an inexpensive alternative to platinum or other noble metals for the electrochemical or photochemical generation of hydrogen from water[10,24–27], which could be a promising clean energy source. The better understanding of catalytical active edge sits of MoS_2 is critical for the advanced catalysts design and developing its practical applications[28]. However, the precise molecular structure modulation and engineering, especially for a well-defined edge site, is fundamentally challenging and rarely reported. On the other hand, noble metal nanoparticles such as Au, Pt and Ag are a class of materials with unique chemical and physical properties which find great applications in biosensing[29,30], photonics[31,32] and catalysis[33,34] It can be expected that the noble metal nanoparticles (NPs) anchored on the MoS_2 sheet could potentially extend its functionalities as novel catalytic, magnetic, and optoelectronic nanomaterials[28,35]. Furthermore, compared with graphene, MoS_2 is a semiconducting material with a suitable band gap around 1.2 to 1.9 eV, depending on its thickness[6,20,21]. It is possible to form *p-n* junctions with other semiconducting materials as new type of electronic devices. While substantial research efforts have been paid, the Fermi level engineering of MoS_2 layers by chemical doping methods are still lack of investigation. It was reported metal NPs can be selectively decorated on carbon nanomatierals by controlling the surface wetting properties[36] and it was also suggested the edges of 2D nanotmateirals may favor the anchoring of metal NPs[37]. However, location dependence of metal NPs decoration on MoS_2 layers

was rarely reported. In this contribution, we study the controllable decoration of isolated MoS_2 single crystal prepared by chemical vapor deposition method (CVD-MoS_2) by Au NPs. The CVD-MoS_2 layers are in well-defined triangular shapes, providing a perfect template for the nanoparticle decoration. It was found that $AuCl_4^-$ ions can be reduced to neutral gold atoms selectively on the edge part, or defective sites of MoS_2 layers by a simple solution dip casting method. The quality of MoS_2-Au NPs composite was evaluated by atomic force microscopy (AFM), transmission electron microscopy (TEM), selected area electron diffraction (SAED), X-ray energy dispersive spectroscopy (EDS), Raman spectroscopy, X-ray photoelectron spectroscopy (XPS) and electrical characterizations.

Results

With the recently developed techniques for MoS_2 growth by CVD method, single layer and crystalline MoS_2 can be produced in a large scale on single crystal substrates[16–18] or even an atomically thin graphene layer[15]. These highly crystalline CVD-MoS_2 layers serve as good model 2D material systems for us to investigate the growth mechanism of Au NPs on 2D materials. Fig. 1 (A) shows the AFM images of the MoS_2 sheets obtained on the sapphire substrates. Smooth surface morphology of MoS_2 sheet is observed under AFM, which suggests that a layer structure of MoS_2 is formed. These continuous MoS_2 layers are formed by small triangular MoS_2 single crystals with a typical thickness of 0.71 nm (See supporting information Figure S1). According to the previous report[38], the triangular shape is a unique feature of the single-layer MoS_2 clusters, since the S edge terminations is considerably more stable. The inset in Fig. 1 (A) displays the non-continuous MoS_2 single crystals in a triangular shape, where the well-defined feature allows us to further study the reactivity of MoS_2 edges and basal planes. Fig. 1(B) provides AFM images of the MoS_2 nanosheets with Au NPs grown on them. The AFM images clearly show that small NPs with a diameter around 5 nm were formed after $AuCl_4^-$ doping and there is no particles found on the surface of substrate which suggests the selectively reduction reaction of $AuCl_4^-$ on MoS_2 nanosheets. Interestingly, the Au NPs tend to form on the edge sites of MoS_2 with only few particles on the basal plane of MoS_2 layers. Previously we report the Au NPs tend to nucleate on the graphene wrinkles due to the morphology change which could trap the precursor and act as the initial nucleation centers for Au particle growth[39]. Different from the chemical vapor deposited graphene (CVD-G), there is no obvious wrinkle formation on CVD-grown MoS_2 nanosheets. The atomically flat surface morphology excludes the influence of different surface energy induced by surface smoothness. In this case, the preferential formation of Au NPs on the edge sites of MoS_2 indicates that the edge site is more reactive than the basal plane region. The edge area could attract the $AuCl_4^-$ precursor at the initial stage, and act as the first nucleation center for Au growth. The intensity of photoluminescence (PL) peak and the energy separation between the Raman A_{1g} and E_{2g} peaks have been found to relate to the number of MoS_2 layers[20,21]. Fig. 1 (C) shows the Raman and PL spectra for the MoS_2 layer, where the excitation light source is a continuous laser with a wavelength of 473 nm. The Raman peaks at 405 and 385.6 cm^{-1} are identified as the A_{1g} and E_{2g} vibration modes, which are characteristics for MoS_2. The PL spectrum displays a distinct main emission peak at ~663 nm, which is in good agreement with the MoS_2 thin layer obtained from exfoliation method. The PL and Raman characterizations suggest the good crystallinity of the CVD-MoS_2.

XPS was applied to reveal the chemical composition of the nano-sized particles. Fig. 2 shows the XPS spectra of the Au doped MoS_2 nanosheets on Sapphire substrates. As shown in Fig. 2 (A) and (B), the Mo 3d shows two peaks at 229.2 eV and 232.3 eV, which can be attributed to the doublet of Mo $3d_{5/2}$ and Mo $3d_{3/2}$. The binding energy for S $2p_{3/2}$ and S $2p_{1/2}$ are 162.0 eV and 163.3 eV, shown in Fig. 2 (B). The Mo and S binding energies are in good agreement with reported value[40], indicating that the doping of Au does not severely change the crystallinity of MoS_2, and the MoS_2 monolayer

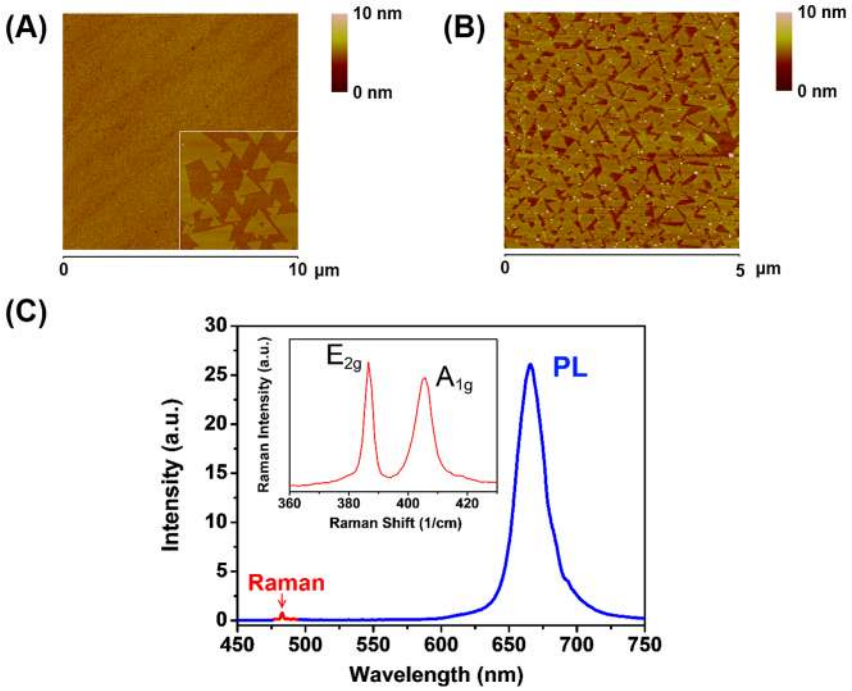

Figure 1 | MoS_2 nano-flakes on *c*-face sapphire substrate substrates. (A) Typical AFM height images of MoS_2 flakes grown on *c*-face sapphire substrates. Inset shows a non-continuous MoS_2 layers formed in triangular feature; (B) AFM image of the corresponding regions after Au nano particles decoration. For these samples, the Au precursor adsorption time was 20 seconds and rinsed with DI water after dip casting; (C) photoluminescence spectra for the obtained CVD-MoS_2 layers, inset shows the Raman spectra of the CVD-MoS_2. Both Raman and PL experiments were performed using a confocal spectrometer with 476 nm excitation laser.

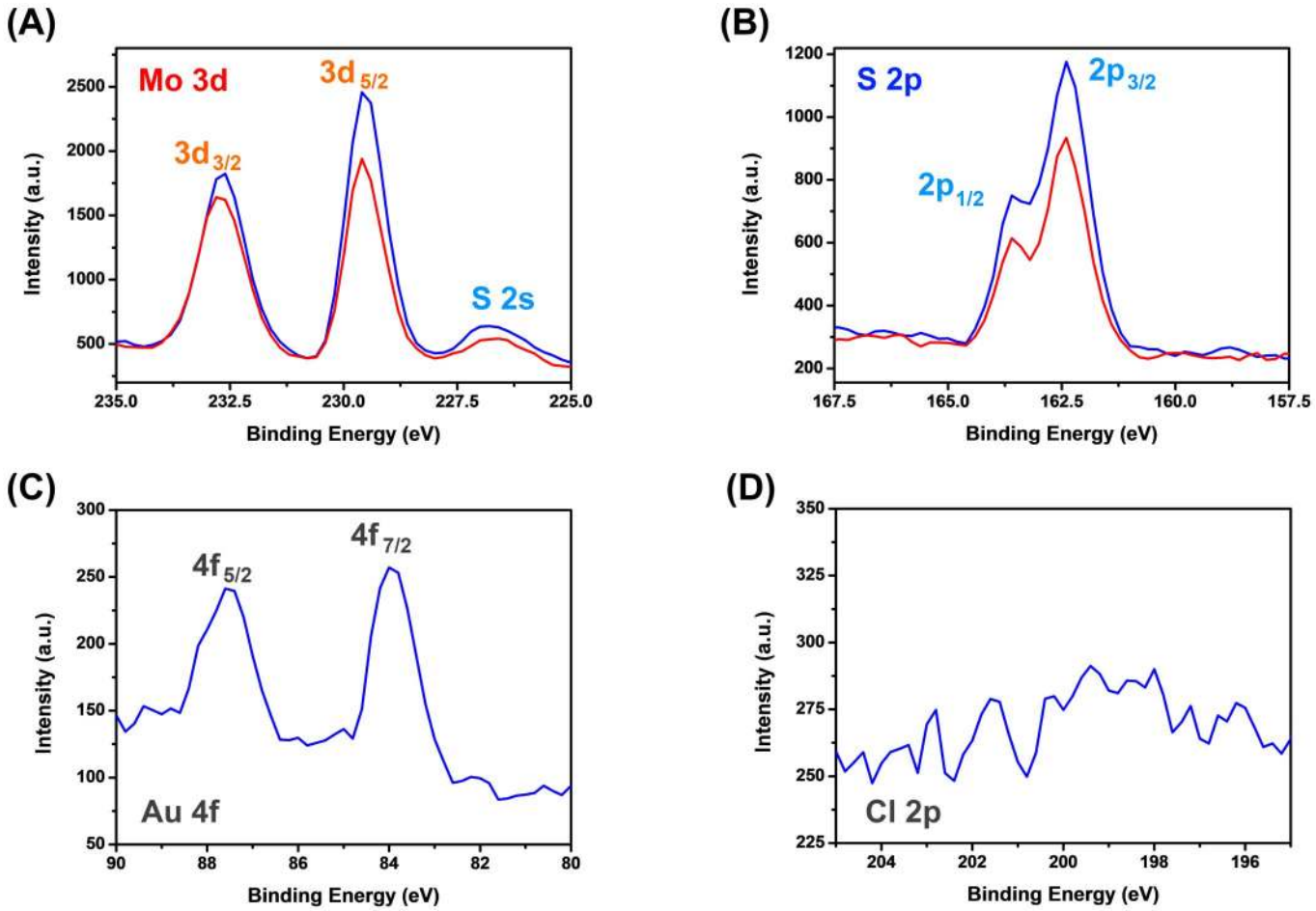

Figure 2 | Chemical composition analysis by X-Ray photoemission spectroscopy (XPS) for (A) Mo, (B) S, (C) Au and (D) Cl binding energies of the MoS_2 layers after Au nanoparticles decoration. The red cure in (A) and (B) display the corresponding spectrum taken from the pristine CVD-MoS_2 sample.

is chemically stable in $HAuCl_4$ aqueous solutions. The XPS scans for the MoS_2 samples after $AuCl_4^-$ doping confirm the chemical bonding states of the MoS_2 layers and Au as displayed in Fig. 2 (C). No detectable Cl signal within the bonding energy ranging from 196 eV to 204 eV has been observed in Fig. 2 (D). This suggested that there is no physical adsorption of $AuCl_4^-$ on MoS_2 surface and $AuCl_4^-$ has been fully reduced to Au. The calculated atomic concentration of Mo, S and Au from XPS are 33.9%, 64.6% and 1.5% with a ratio of 1 : 1.90 : 0.044.

To explore the location dependency of Au NPs growth on MoS_2 layers and understand the tendency of the epitaxial stacking manner of Au NPs on MoS_2 nanosheets, the Au NPs/CVD-MoS_2 was investigated by analyzing the high resolution TEM (HRTEM) and the corresponding fast Fourier transform (FFT) images. The results were also compared with the Au doped chemical exfoliated MoS_2 (Au NPs/CE-MoS_2) which has a higher defect density.

Fig. 3 (A) and (B) are the TEM images of Au NPs/CVD-MoS_2, triangular nanosheets with well-proportioned NPs along the edge and sporadic ones on the surface region which is in good consistence with the AFM results. As observed in Fig. 3 (B), NPs appeared to be darker in contrast when compared to that of the MoS_2 nanosheets. We noticed that due to the low content of gold in the CVD-MoS_2 nanosheets, no Au element can be obviously detected in Au NPs/CVD-MoS_2 according to EDS (see supporting information Figure S2). Fig. 3 (C) displays a HRTEM image taken from the edge part of Au NPs/CVD-MoS_2. The inset shows the SAED pattern from the surface of CVD-MoS_2, which can be attributed to the 2H-MoS_2 single crystal[15,16,18,19]. For the SAED analysis, in order to avoid cover more than one piece of triangular MoS_2 flake, the aperture in TEM analysis was set to be 10 μm (with the electron beam size of 150 nm), which is a bit smaller than that of the Au decorated MoS_2 flakes. Fig. 3 (D) depicts the HRTEM image of an Au NP which

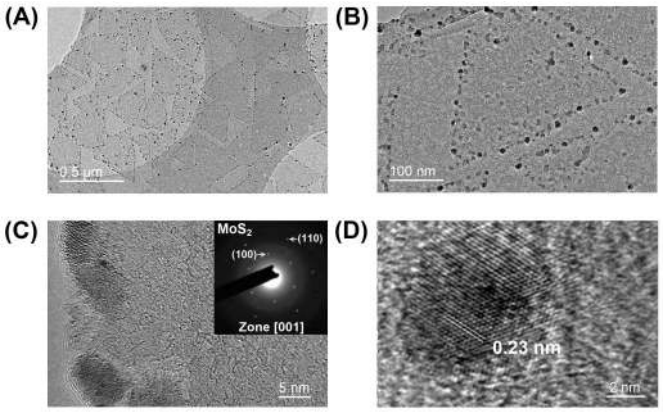

Figure 3 | TEM images of the Au NPs decorated CVD-MoS_2 nano-flakes. (A) Low magnification TEM image of isolated single crystal MoS_2 flakes in triangular shape. (B) A zoomed-in TEM image of MoS_2 flakes with nano-size particles mostly adsorbed on the edge parts. (C) A typical HRTEM image taken from the edge of a MoS_2 flake. Inset shows the SAED pattern from the MoS_2 surface. (D) shows an enlarged HRTEM image of Au NPs on MoS_2 edge, the measured d spacing distance is around 0.23 nm.

clearly reveals a single crystal nature of Au nano-domain. The measured *d* spacing is around 0.23 nm which is in good consistence with the Au (111) spacing[41]. We also noticed although it is hard to indicate the grain boundaries of continuous CVD-MoS_2 layer, after Au decoration and rinsing process, part of the MoS_2 film could break and left mechanically formed MoS_2 edges (See supporting information Figure S3). The Au NPs tend to form on the exposed MoS_2 edges rather than on the basal plane region of MoS_2. These observations align well and suggest that the MoS_2 defects, especially for the edge area, may be more reactive than the basal surface.

In order to further examine the assumption regarding the relationship between Au NPs and the defects in MoS_2, MoS_2 films were also prepared by chemical exfoliation (CE-MoS_2) method and characterized by TEM. The chemical exfoliation method involves lithium ion intercalation between MoS_2 layers and ultra-sonication was applied to assist the further exfoliation of MoS_2 layers and forming few layer or monolayer MoS_2 nanosheets, therefore CE-MoS_2 was expected to possess more defects than the CVD-MoS_2. The HRTEM taken for CE-MoS_2 suggest that the CE-MoS_2 films exhibit poor crystallinity compared to the CVD-MoS_2 as expected. (See supporting materials Figure S4). Fig. 4 (A) and (B) displays the TEM image of the chemically exfoliated MoS_2 film after Au doping. Dramatically different from the CVD-MoS_2, both large and small Au NPs can be found on CE-MoS_2 as shown in Fig. 4 (A) and 4 (B). The particle density is also much higher than that observed from CVD-MoS_2. The inset images in Fig. 4 (B) shows the corresponding SAED images. The SAED image of a typical Au NPs decorated CE-MoS_2 film exhibits three distinguished rings which can be assigned to the MoS_2 {100}, {110} and Au {111} planes with lattice spacing of 0.27, 0.16 and 0.23 nm respectively. The characteristic electron diffraction ring assigned to the {111} planes of the face-centred-cubic (fcc) lattice of Au is much sharper and stronger in comparison with the other planes, revealing the predominant orientation of the Au {111} planes. The increase of Au NPs density on CE-MoS_2 strongly suggests that the forming of Au NPs is associated with the defects of MoS_2. The edge parts or defects in MoS_2 layers could interact with the $AuCl_4^-$ precursor at the initial stage, and act as the first nucleation center for Au NPs growth, therefore the results suggest the Au NPs could effectively work as a defect marker for MoS_2 layers. HRTEM images were taken to further investigate the orientation relationship between MoS_2 film and Au particles Fig. 4 (C) and (D) show the HRTEM images of typical Au NPs on CE-MoS_2 with different particle sizes ranging from ~2 nm to ~10 nm. The HRTEM image in Fig. (D) displays an in plane lattice spacing of 0.23 nm which is in good agreement with the number of Au (111). Although it is not easy to determine the accurate lattice of CE-MoS_2 due to its defective polycrystalline nature, the SEAD and HRTEM results suggest that the defective sites in MoS_2 layers could effectively attract Au NPs precursor and serve as nucleation sites and the surface plane of MoS_2 serves as a growth temple for Au NPs along its {111} plane. It was previously reported single layer MoS_2 nano-islands can form on crystalline Au (111) surfaces with their (0001) basal plane oriented parallel to the Au (111) substrate surface[38]. In this study, we propose at the very beginning, the $AuCl_4^-$ ions adsorb onto the defective sites in MoS_2 layers and reduced to Au atoms which subsequently form Au nanoclusters, therefore the density of Au NPs depends on the defect density of MoS_2 layer. Meanwhile, the Au {111} has the lowest surface energy[42,43] and small lattice mismatch with MoS_2 (0001), which promotes the preferential orientation of Au (111) crystal planes on MoS_2 surface.

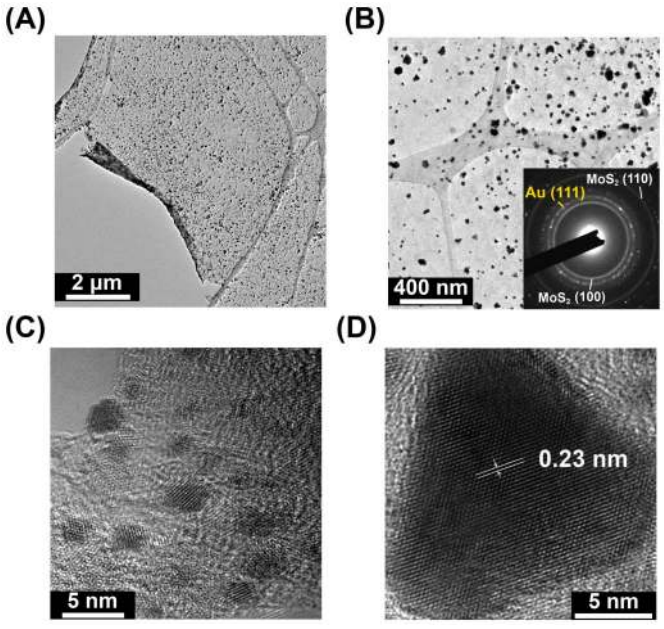

Figure 4 | TEM images of the Au NPs/CE-MoS_2 film. (A) Low magnification TEM image of Au NPs/CE-MoS_2 film. (B) Enlarged TEM image of Au NPs/CE-MoS_2 film with various Au NPs size. The inset shows the SAED pattern from the film.) (C) A typical HRTEM image of small particle (~2 nm) located on the CE-MoS_2 films; (D) HRTEM image of large Au particle (~10 nm) located on the CE-MoS_2.

Discussion

Various research methods have been developed aiming at tuning the electronic properties of 2D materials. According to our previous report[39,44], the work function of graphene layer can be effectively controlled by immersing graphene film in $AuCl_4^-$ solution, due to the spontaneous reduction of Au^{3+} to Au^0. Raman spectroscopy is a powerful nondestructive characterization tool to reveal the level of doping in single-layer MoS_2 due to the strong electron-phonon interaction[45,46]. It has been reported that *n*-doping results in softening of the A_{1g} phonon which results in decrease of relative intensity and peak frequency difference between A_{1g} and E_{2g} modes[46] while *p*-doping in MoS_2 layers should cause relative shifting of the Raman-active modes in opposite direction. Figure 5 (A) shows typical Raman spectra for a single layer MoS_2 sheet before and after Au NPs decoration. The MoS_2 layer exhibits two Raman characteristic bands at ~404 and 386 cm^{-1}, corresponding to the A_{1g} and E_{2g} modes respectively. It was reported oxygen in the ambient may attack Mo-S-Mo bands and cause the shift of Raman vibrations modes[45]. To reduce the influence from the ambient oxygen, the Raman spectra were taken right after the CVD synthesis and/or Au NPs decoration. It was also noticed that the Raman spectra shows some variation across the sample surface, therefore to reveal the doping effect of Au NPs a set of data points were taken and statistical analysis were carried out as shown in Figure 5 (B) and (C). Figure 5(B) and (C) compare the relative peak intensity and frequency difference shift of A_{1g} and E_{2g} Raman modes, respectively. The results showing a detectable upshift of A_{1g} frequency and an increase of A_{1g}/E_{2g} peak intensity ratio, which suggest distinct *p*-doping caused by Au NPs decoration[45,46]. To further evaluate doping effect of Au NPs on CVD-MoS_2 electrically, top-gate transistors were fabricated by evaporating Au/Ti electrodes directly on top of the MoS_2 layers on sapphire substrate. The MoS_2 electric double-layer transistors (EDLTs)[47,48] were formed with an ionic gel film which works as dielectric layer for the transistor. Details of device fabrication can be found in the previous report[48]. It is worthy to mention, since the devices are directly fabricated on the growth substrates and no transfer process is involved, the intrinsic transport properties of CVD-MoS_2 layers and the effect of Au NPs on the transistor performance can be directly accessed. Fig. 5 (D) shows the transfer curve of CVD-MoS_2 EDLTs before and after Au NPs decoration. Supporting information Figure S5 shows the I-V_g curves plotted in log scale.

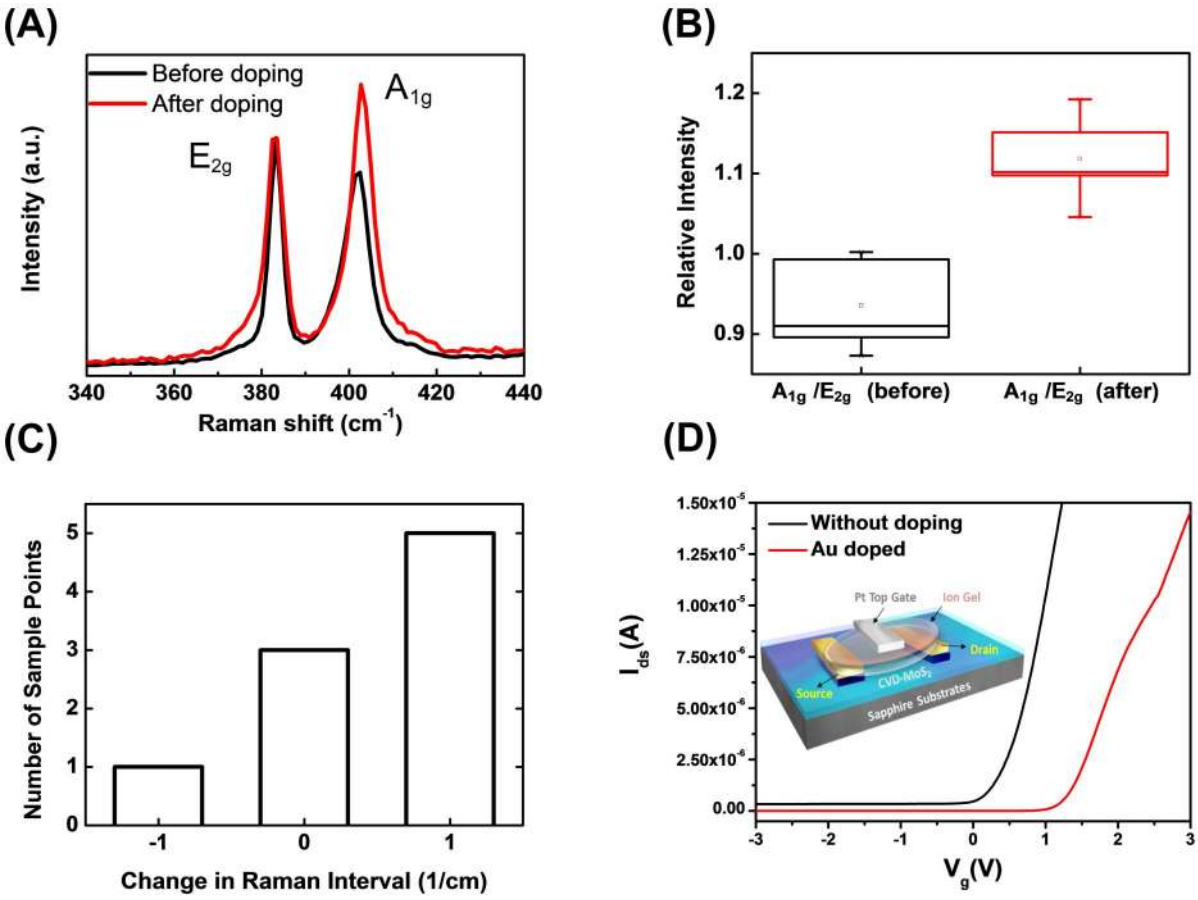

Figure 5 | (A) Typical Raman spectra of MoS_2 sheets before and after Au NPs decoration; (B) and (C) show the statistical analysis of the relative intensity and frequency change in E_{2g} and A_{1g} vibration mode induced by the Au NPs decoration; (D) Thin-film MoS_2 EDLT constructed with an ion gel dielectric layer. Black and red lines correspond to the transfer characteristics of the MoS_2 EDLT before and after Au NPs decoration. The inset schematically illustrates the device structure, the source and drain electrodes were electrically isolated from the ion gel by a thin PDMS layer.

The pristine CVD-MoS_2 EDLTs show typical transfer curves of n-typed behavior which is consistent with the other reports. Au/Ti (80 nm and 5 nm, respectively) were used as the source/drain electrodes. The work function of Ti is closer to the conduction band edge of MoS_2 and results an expected *n*-typed behaviors. After Au NPs decoration, the threshold gate voltage changes from 0.47 V to 1.29 V and the transfer curve shifts to the right hand side which indicates that a *p*-doing effect has been introduced by the Au NPs. The electrical results are consistent with the Raman characterizations confirming that the $AuCl_4^-$ ions in solution can strongly withdraw electrons from MoS_2 layers and reduces to Au NPs, therefore, it is anticipated for a down shift of Fermi level in MoS_2 layers. It is found that the on/off ratio for the device after Au NPs doing is around 3.54×10^3, which is around 50 times larger than that of the pristine MoS_2 electric double-layer transistors (EDLT). The measured maximum current for the doped and pristine MoS_2 EDLT is 13.7 mA and 22.5 mA, respectively. The mobility of the MoS_2 EDLT can be derived from the slope of the transfer characteristics using the standard equation $I_d = (\mu W V_D C_i/L)(V_G\text{-}V_{th})$ for the linear region[48]. Where I_d is the drain current, μ is the field-effect mobility, W is the channel width, V_D is the drain voltage, C_i is the specific capacitance of the dielectric, L is the channel length, V_G is the gate voltage, and V_{th} is the threshold voltage. From the calculation, the mobility for Au NPs doped MoS_2 is around 2.44 $cm^2/(Vs)$, which is 2 times smaller than the pristine MoS_2 EDLT.

In conclusion, we have proposed a simple method to decorate the CVD-MoS_2 and CE-MoS_2 thin layers with Au NPs. AFM, TEM, XPS characterization methods were carried out to investigate the growth mechanism and epitaxial stacking manner of Au NPs and MoS_2. The Au NPs exhibited a remarkable *p*-doping effect to the MoS_2 transistors . Hence, the proposed Au NPs decoration method can provide promising nanomaterials hybrids for the application of future optoelectronics devices.

Methods

CVD-MoS_2 synthesis. CVD-MoS_2 was prepared using the method High-crystal-quality MoS_2 were grown on a sapphire substrates by chemical vapor deposition method inside a horizontal tube furnace. The detailed fabrication procedure can be found elsewhere[17,18]. To be brief, the MoS_2 films were synthesized on c-face sapphire substrates in a hot-wall furnace. High purity MoO_3 (99%, Aldrich) and S powder (99.5, Alfa) were placed in two separated Al_2O_3 crucibles and the substrates were placed on the downstream side of the Ar carrying gas. The MoS_2 samples were obtained by annealing at 650°C for 15 min with a hearting rate of 15°C/min and Ar flow rate was kept at 1 sccm.

Chemical exfoliated MoS_2. The MoS_2 nanoflakes was obtained by lithium intercalation method follow the procedure reported before[20]. 0.5 g of natural MoS_2 crystals from Sigma-Aldrich was dispersed in 5 mL of 1.6 M butyllithium solution in hexane (Sigma-Aldrich) for 48 hours in a flask filled with argon gas. The Li_xMoS_2 was retrieved by filtration and washed with hexane (60 mL) to remove excess lithium and organic residues. Exfoliation was achieved by ultrasonicating the obtained Li_xMoS_2 slurry in DI-water for 1 h. The mixture was centrifuged and re-dispersed in DI water for at least 5 times to remove excess lithium in the form of LiOH and unexfoliated material. Thin films were prepared by filtering through a mixed cellulose ester membrane with 0.025 μm pores (Millipore). The film was delaminated on water surface for subsequent transfer onto substrates or TEM Grids.

Au NPs decoration on CVD-MoS_2 and CE-MoS_2. $AuCl_3$ dissolved in water was used for the growth of Au nano particles (Au NPs) on MoS_2. To prepare Au NPs/CVD-MoS_2, the as prepared CVD-MoS_2 on sapphire substrates was directly

immersed in 5 mM $AuCl_3$ for 20 sec, followed by gently rinsing with DI water. To prepare Au NPs/CE MoS_2 samples, the CE MoS_2 film was firstly delaminated on water surface by the previously described method[20]. Several drops of 5 mM $AuCl_3$ water solution were added into the water subsequently. Finally, the Au NPs/CE-MoS_2 floating on water surface can be picked up by TEM grids or arbitrary substrates.

Transfer of the as-grown Au NPs/MoS_2 hybrid to arbitrary substrates. The CVD-MoS_2 and Au NPs decorated MoS_2 films was transferred by coating the film with a thin layer (~100 nm) of Poly[methylmethacrylate] (PMMA). After etching the underlying sapphire substrates with KOH aquariums (with a concentration of 2 M) at 80°C, the PMMA/MoS_2 film was transferred to DI water and was suspended on the surface of water to remove the etchant residue. Subsequently, the film can be transferred to any substrate or TEM grids for analysis and characterization. Finally, the top layer of PMMA can be removed by acetone or by directly annealing the samples in an Ar and H_2 atmosphere at 400°C for 2 hours.

Characterizations. Surface morphology of the samples was examined with commercial atomic force microscope (AFM, Veeco Icon). Raman spectra were collected in a NT-MDT confocal Raman microscopic system with exciting laser wavelength of 473 nm and the laser spot-size is around 0.5 μm. For the Raman characterization, the Si peak at 520 cm^{-1} was used as reference for wavenumber calibration. Field-emission transmission electron microscope (JEOL JEM-2010F, operated at 200 keV), equipped with an energy dispersive spectrometer (EDS) was used to obtain the information of the microstructures and the chemical compositions. Chemical composition was determined by X-ray photoelectron spectroscope (XPS, Phi V5000). XPS measurements were performed with an Al Kα X-ray source. The energy calibrations were made against the C 1s peak to eliminate the charging of the sample during analysis.

1. Geim, A. K. & Novoselov, K. S. The rise of graphene. *Nat Mater* **6**, 183–191 (2007).
2. Novoselov, K. S. *et al.* Two-dimensional gas of massless Dirac fermions in graphene. *Nature* **438**, 197–200 (2005).
3. Novoselov, K. S. *et al.* Electric Field Effect in Atomically Thin Carbon Films. *Science* **306**, 666–669 (2004).
4. Kubota, Y., Watanabe, K., Tsuda, O. & Taniguchi, T. Deep Ultraviolet Light-Emitting Hexagonal Boron Nitride Synthesized at Atmospheric Pressure. *Science* **317**, 932–934 (2007).
5. Dean, C. R. *et al.* Boron nitride substrates for high-quality graphene electronics. *Nat Nano* **5**, 722–726 (2010).
6. Radisavljevic, B., Radenovic, A., Brivio, J., Giacometti, V. & Kis, A. Single-layer MoS_2 transistors. *Nat Nano* **6**, 147–150 (2011).
7. Lembke, D. & Kis, A. Breakdown of High-Performance Monolayer MoS_2 Transistors. *ACS Nano* **6**, 10070–10075 (2012).
8. Wang, H. *et al.* Integrated Circuits Based on Bilayer MoS_2 Transistors. *Nano Lett* **12**, 4674–4680 (2012).
9. Chang, Y.-H. *et al.* Highly Efficient Electrocatalytic Hydrogen Production by MoS_x Grown on Graphene-Protected 3D Ni Foams. *Adv Mater* **25**, 756–760 (2013).
10. Li, Y. *et al.* MoS_2 Nanoparticles Grown on Graphene: An Advanced Catalyst for the Hydrogen Evolution Reaction. *J Am Chem Soc* **133**, 7296–7299 (2011).
11. Kong, D. *et al.* Synthesis of MoS_2 and $MoSe_2$ Films with Vertically Aligned Layers. *Nano Lett* **13**, 1341–1347 (2013).
12. Mak, K. F., Lee, C., Hone, J., Shan, J. & Heinz, T. F. Atomically Thin MoS_2: A New Direct-Gap Semiconductor. *Physical Review Letters* **105**, 136805 (2010).
13. Coleman, J. N. *et al.* Two-Dimensional Nanosheets Produced by Liquid Exfoliation of Layered Materials. *Science* **331**, 568–571 (2011).
14. Gordon, R. A., Yang, D., Crozier, E. D., Jiang, D. T. & Frindt, R. F. Structures of exfoliated single layers of WS_2, MoS_2, and $MoSe_2$ in aqueous suspension. *Physical Review B* **65**, 125407 (2002).
15. Shi, Y. *et al.* van der Waals Epitaxy of MoS_2 Layers Using Graphene As Growth Templates. *Nano Lett* **12**, 2784–2791 (2012).
16. Liu, K.-K. *et al.* Growth of Large-Area and Highly Crystalline MoS_2 Thin Layers on Insulating Substrates. *Nano Lett* **12**, 1538–1544 (2012).
17. Lin, Y.-C. *et al.* Wafer-scale MoS_2 thin layers prepared by MoO_3 sulfurization. *Nanoscale* **4**, 6637-6641 (2012).
18. Lee, Y.-H. *et al.* Synthesis of Large-Area MoS_2 Atomic Layers with Chemical Vapor Deposition. *Adv Mater* **24**, 2320–2325 (2012).
19. Zhan, Y., Liu, Z., Najmaei, S., Ajayan, P. M. & Lou, J. Large-Area Vapor-Phase Growth and Characterization of MoS_2 Atomic Layers on a SiO_2 Substrate. *Small* **8**, 966–971 (2012).
20. Eda, G. *et al.* Photoluminescence from Chemically Exfoliated MoS_2. *Nano Lett* **11**, 5111–5116 (2011).
21. Splendiani, A. *et al.* Emerging Photoluminescence in Monolayer MoS_2. *Nano Lett* **10**, 1271–1275 (2010).
22. Brivio, J., Alexander, D. T. L. & Kis, A. Ripples and Layers in Ultrathin MoS_2 Membranes. *Nano Lett* **11**, 5148–5153 (2011).
23. Laursen, A. B., Kegnaes, S., Dahl, S. & Chorkendorff, I. Molybdenum sulfides-efficient and viable materials for electro - and photoelectrocatalytic hydrogen evolution. *Energy & Environmental Science* **5**, 5577–5591 (2012).
24. Chen, Z. *et al.* Core–shell MoO_3–MoS_2 Nanowires for Hydrogen Evolution: A Functional Design for Electrocatalytic Materials. *Nano Lett* **11**, 4168–4175 (2011).
25. Zong, X. *et al.* Photocatalytic H_2 Evolution on MoS_2/CdS Catalysts under Visible Light Irradiation. *The Journal of Physical Chemistry C* **114**, 1963–1968 (2010).
26. Bonde, J., Moses, P. G., Jaramillo, T. F., Norskov, J. K. & Chorkendorff, I. Hydrogen evolution on nano-particulate transition metal sulfides. *Faraday Discuss* **140**, 219–231 (2009).
27. Zhou, W. *et al.* Synthesis of Few-Layer MoS_2 Nanosheet-Coated TiO_2 Nanobelt Heterostructures for Enhanced Photocatalytic Activities. *Small* **9**, 140–147 (2013).
28. Jaramillo, T. F. *et al.* Identification of Active Edge Sites for Electrochemical H_2 Evolution from MoS_2 Nanocatalysts. *Science* **317**, 100–102 (2007).
29. Dong, X., Shi, Y., Huang, W., Chen, P. & Li, L.-J. Electrical Detection of DNA Hybridization with Single-Base Specificity Using Transistors Based on CVD-Grown Graphene Sheets. *Adv Mater* **22**, 1649–1653 (2010).
30. He, S. *et al.* Graphene-Based High-Efficiency Surface-Enhanced Raman Scattering-Active Platform for Sensitive and Multiplex DNA Detection. *Anal Chem* **84**, 4622–4627 (2012).
31. Qian, H., Zhu, Y. & Jin, R. Atomically precise gold nanocrystal molecules with surface plasmon resonance. *Proceedings of the National Academy of Sciences*. DOI 10.1073/pnas.1115307109 (2012).
32. Huang, F. & Baumberg, J. J. Actively Tuned Plasmons on Elastomerically Driven Au Nanoparticle Dimers. *Nano Lett* **10**, 1787–1792 (2010).
33. Lu, Y.-C. *et al.* Platinum−Gold Nanoparticles: A Highly Active Bifunctional Electrocatalyst for Rechargeable Lithium−Air Batteries. *J Am Chem Soc* **132**, 12170–12171 (2010).
34. Murdoch, M. *et al.* The effect of gold loading and particle size on photocatalytic hydrogen production from ethanol over Au/TiO_2 nanoparticles. *Nat Chem* **3**, 489–492 (2011).
35. Huang, X. *et al.* Solution-phase epitaxial growth of noble metal nanostructures on dispersible single-layer molybdenum disulfide nanosheets. *Nat Commun* **4**, 1444 (2013).
36. Yick, S., Han, Z. J. & Ostrikov, K. Atmospheric microplasma-functionalized 3D microfluidic strips within dense carbon nanotube arrays confine Au nanodots for SERS sensing. *Chem Commun* **49**, 2861–2863 (2013).
37. Rider, A. E., Kumar, S., Furman, S. A. & Ostrikov, K. Self-organized Au nanoarrays on vertical graphenes: an advanced three-dimensional sensing platform. *Chem Commun* **48**, 2659–2661 (2012).
38. Helveg, S. *et al.* Atomic-Scale Structure of Single-Layer MoS_2 Nanoclusters. *Phys Rev Lett* **84**, 951–954 (2000).
39. Kim, K. K. *et al.* Enhancing the conductivity of transparent graphene films via doping. *Nanotechnology* **21**, 285205 (2010).
40. Baker, M. A., Gilmore, R., Lenardi, C. & Gissler, W. XPS investigation of preferential sputtering of S from MoS2 and determination of MoS_x stoichiometry from Mo and S peak positions. *Appl Surf Sci* **150**, 255–262 (1999).
41. Huang, X. *et al.* Synthesis of hexagonal close-packed gold nanostructures. *Nat Commun* **2**, 292 (2011).
42. Chen, M., Wu, B., Yang, J. & Zheng, N. Small Adsorbate-Assisted Shape Control of Pd and Pt Nanocrystals. *Adv Mater* **24**, 862–879 (2012).
43. Wang, A.-J. *et al.* Melamine assisted one-pot synthesis of Au nanoflowers and their catalytic activity towards p-nitrophenol. *New J Chem* **36**, 2286–2291 (2012).
44. Shi, Y. *et al.* Work Function Engineering of Graphene Electrode via Chemical Doping. *Acs Nano* **4**, 2689–2694 (2010).
45. Li, H. *et al.* From Bulk to Monolayer MoS_2: Evolution of Raman Scattering. *Adv Funct Mater* **22**, 1385–1390 (2012).
46. Chakraborty, B. *et al.* Symmetry-dependent phonon renormalization in monolayer MoS_2 transistor. *Phys Rev B* **85**, 161403 (2012).
47. Braga, D., Gutiérrez Lezama, I., Berger, H. & Morpurgo, A. F. Quantitative Determination of the Band Gap of WS2 with Ambipolar Ionic Liquid-Gated Transistors. *Nano Lett* **12**, 5218–5223 (2012).
48. Pu, J. *et al.* Highly Flexible MoS_2 Thin-Film Transistors with Ion Gel Dielectrics. *Nano Lett* **12**, 4013–4017 (2012).

Acknowledgements

This work is supported by SUTD-MIT international design center fund to Dr Yang Hui Ying. L.J. Li thanks the support from Academia Sinica (IAMS and Nano program) and National Science Council Taiwan (NSC-99-2112-M-001-021-MY3).

Author Contributions

Y. Shi and H.Y. Yang conceived and designed the study. Y. Shi and H.Y. Yang wrote the manuscript. Y. Shi, J. Huang and L. Jin performed the experiments. Y. Hsu helped to do the experiments. L.J. Li and S.F. Yu gave scientific advice. All the authors contributed to discussion and reviewed the manuscript.

Additional information

Supplementary information accompanies this paper at http://www.nature.com/scientificreports

Competing financial interests: The authors declare no competing financial interests.

How to cite this article: Shi, Y. *et al.* Selective Decoration of Au Nanoparticles on Monolayer MoS_2 Single Crystals. *Sci. Rep.* **3**, 1839; DOI:10.1038/srep01839 (2013).